Colloids and Surfaces A: Physicochem. Eng. Aspects 392 (2011) 256–263

Contents lists available at SciVerse ScienceDirect

Colloids and Surfaces A: Physicochemical and Engineering Aspects

journal homepage: www.elsevier.com/locate/colsurfa

On the interaction of encapsulated pH indicator species within a silica matrix produced by three sol–gel routes

Larissa Brentano Capeletti[a], Claudio Radtke[a], João Henrique Z. Dos Santos[a,*], Edwin Moncada[b], Zenis N. Da Rocha[c], Iuri Muniz Pepe[d]

[a] Instituto de Química, UFRGS, Av. Bento Gonçalves, 9500 Porto Alegre, Brazil
[b] Instituto Tecnológico Metropolitano, Robledo, Calle 73 # 76 A 354, bloque F, Medellín, Colombia
[c] Instituto de Química, Universidade Federal da Bahia, Campus de Ondina, 40170-290 Salvador, BA, Brazil
[d] Instituto de Física, Universidade Federal da Bahia, Campus de Ondina, 40210-340 Salvador, BA, Brazil

ARTICLE INFO

Article history:
Received 7 August 2011
Received in revised form 1 October 2011
Accepted 4 October 2011
Available online 12 October 2011

Keywords:
Sensor
Sol–gel
Encapsulation
Network interaction
Voltammetry

ABSTRACT

Solid acid–base sensors were prepared by encapsulating two pH indicators (brilliant yellow or acridine) within a silica matrix by the sol–gel method using three different routes: (1) non-hydrolytic, (2) acid catalyzed and (3) base catalyzed. The interactions of the silica-indicator with the resulting materials were then investigated by cyclic and differential pulse voltammetry. Complementary, ultraviolet–visible, photoacoustic spectroscopy was employed for the characterization of the interactions by monitoring the band shifts (bathochromic or hypsochromic, depending on the sol–gel route) between the neat pH indicators and those encapsulated within the silica network. Furthermore, X-ray photoelectron spectroscopy showed that the N 1s binding energy in brilliant yellow was shifted for the material resulting from the acid route. The electrochemical behavior and the pH indicator interactions with the silica network were dependent on the nature of the employed sol–gel route. For the sensors prepared with acridine, the interactions with the silica network took place through the nitrogen group from the pyridinic ring. For the brilliant yellow indicator, different behaviors were observed depending on the route, suggesting different processes during preparation or analysis. For the basic catalyzed and non-hydrolytic routes, it was not possible to assign a specific interaction. Nevertheless, it seemed that interactions might have taken place through the hydroxyl and/or sulphonic groups. Furthermore, for the brilliant yellow sensor prepared through the acid route, it was possible to show that the interaction probably or partially occurred through the azo groups.

1. Introduction

A common method for preparing optical sensors is by the immobilization of the receptor element within a matrix of interest, and the choice of matrix is dependent upon the sensor application itself. For this goal, the sol–gel process has been successfully employed due to its singular versatility and the following characteristics: optic transparency, mechanic stability, chemical resistance and flexibility of sensor morphological configurations [1–3]. In addition, this kind of matrix is permeable to analytes, while keeping the receptor element incorporated inside. Furthermore, this process allows for the possibility of tuning matrix characteristics according to the application that is being used [4,5]. In the case of acid–base sensors, an important feature is the receptor element leaching resistance behavior of the material, especially for continuous monitoring sensors. For this purpose, it is important that a strong interaction between the receptor element and the silica network occurs. However, immobilization or encapsulation methods always require a commitment between non-leaching and maintenance of the activity of the sensor [6].

Acid–base sensors have usually been prepared from pH indicators that have been encapsulated by the sol–gel method [4,7,8]. This kind of sensor has been extensively investigated to improve its performance in terms of response time, durability, sensibility and response range. For such purposes, several properties, such as spectrum shifts, sensible pH range shifts, cyclic repeatability, leaching, response rates and isosbestic points, have been described in the literature [8–11]. These aspects have been exploited as criteria for evaluating the modifications and improvements applied to the sol–gel route, which, in turn, may affect the performance of the pH indicator when encapsulated within the silica matrix. The interactions between silica and the indicator molecules are normally increased by the presence of functional groups on the pH indicators such as hydroxyl, methyl or carbonyl with the hydroxyl

* Corresponding author. Tel.: +55 513 316 7238; fax: +55 513 316 7304.
E-mail address: jhzds@iq.ufrgs.br (J.H.Z. Dos Santos).

0927-7757/$ – see front matter © 2011 Elsevier B.V. All rights reserved.
doi:10.1016/j.colsurfa.2011.10.002

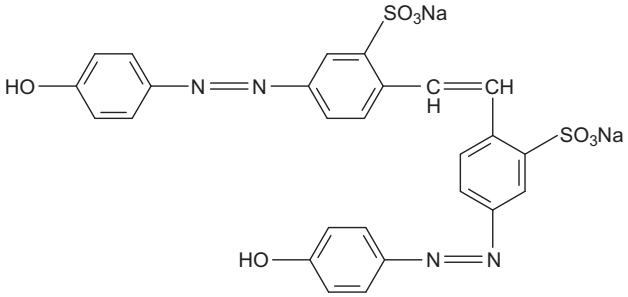

Brilliant yellow

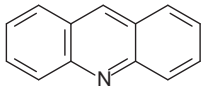

Acridine

Scheme 1. Structure of the investigated pH indicators.

or chemical groups of the silica network [10,12]. For example, some studies have reported the use of chemically modified silicas that can increase the interaction with the receptor elements, therefore, decreasing leaching problems. However, an increase in the response time once the pH indicator was more committed to an interaction with the silica network, thus, hindering the reaction with the analytes, has also been reported [9,13–15].

Taking into account the wide variation and dependence of the obtained sensors as a function of the sol–gel route, we have previously studied the influence of three different sol–gel routes on acid–base sensors [4]. The employed routes tested were the following: acid catalyzed, basic catalyzed and non-hydrolytic, and the tested pH indicators were as follows: alizarin red, brilliant yellow and acridine. The structure of the obtained materials was well characterized, but the interactions between the silica network and the pH indicators were not investigated. Attempts to evaluate them failed due to the low content of encapsulated indicator, which made routine techniques such as infrared spectroscopy not suitable for this evaluation. A good strategy to overcome such constraints was the use of cyclic voltammetry, which has been shown to be very effective in the description of alizarin red performance [16].

Therefore, in the present study, we report the electrochemical behavior of brilliant yellow (BY) and acridine (AC) (Scheme 1), as a function of the pH, and their interactions with the silica network. These interactions were generated through encapsulation by three sol–gel processes: the hydrolytic acid catalyzed route (AR), the hydrolytic basic catalyzed route (BR) and the non-hydrolytic route (NHR) sol–gel processes. The resulting systems were characterized by cyclic voltammetry (CV), differential pulse voltammetry (DPV) and, complementarily, by ultraviolet–visible photoacoustic spectroscopy (UV-PAS) and X-ray photoelectron spectroscopy (XPS). This was done in order to evaluate the behaviors of the pH indicators in the silica networks that had been created by the three different methods, which might influence the electroactivity and/or the interactions between the silica and indicator as a function of different conditions (*i.e.*, pH synthesis and hydrolytic or non-hydrolytic medium).

2. Materials and methods

2.1. Materials

Tetraethoxisilane ($Si(OCH_2CH_3)_4$, TEOS, Merck, >98%) and silicon tetrachloride ($SiCl_4$, Sigma–Aldrich, 99%) were used as received. The acid–base indicators brilliant yellow (BY, 70%) and acridine (AC, 97%) were provided by Sigma Aldrich. Chloridric acid (HCl, Nuclear, 38%), ammonium hydroxide (NH_4OH, Nuclear, 29%) and iron(III) chloride ($FeCl_3$, Merck, 98%) were employed as catalysts. High-purity grade graphite was provided by Fisher Scientific, and buffer solutions were prepared using sodium tetrafluoroborate ($NaBF_4$, Aldrich, 98%), glacial acetic acid (CH_3COOH, Merck, 100%), phosphoric acid (H_3PO_4, Merck, 85%) and boric acid (H_3BO_3, Merck, 99.9%).

2.2. Synthesis of sensors by sol–gel process

Three different routes were employed to prepare the sensors by the sol–gel process using TEOS as the raw material, and these procedures were performed as described in the literature [17–19]. The employed acid–base indicators were brilliant yellow (BY) and acridine (AC), and the three utilized routes were labeled as follows: acid catalyzed route (AR), base catalyzed route (BR) and non-hydrolytic route (NHR). The acid route was catalyzed by chloridric acid (1:20 (HCl:TEOS) ratio) [17], and the basic route was catalyzed by ammonium hydroxide (1:1 (NH_4OH:TEOS) ratio) [19]. The non-hydrolytic route utilized TEOS and $SiCl_4$ and was catalyzed by $FeCl_3$ (0.5 wt.% of the final product weight) [18]. The amount of acidic or basic indicators was 0.1 mol.% of the total amount of alkoxide groups.

The sensors (powder) obtained by the acid or basic routes were prepared using aqueous or ethanolic solutions of the acid–base indicators, respectively, to which catalyst and TEOS were added with stirring at room temperature. The resulting solution was stirred further until gelation (ca. 4 h for the acid route) or until precipitation followed by one additional hour of stirring (total of 1 h and 15 min for the basic route). For the non-hydrolytic route, all procedures were carried out under inert atmosphere. First, the catalyst and the indicator were contacted, and this was followed by the addition of TEOS and $SiCl_4$. The resulting solution was stirred at 80 °C until gelation (ca. 2 h). All solids were milled, washed with water and ethanol and then dried at 110 °C for 12 h. For each route, a corresponding blank (silica without the encapsulation of the pH indicators BY and AC) was prepared.

Thereafter, the resulting sensors were labeled according to the sol–gel route. For example, AL stands for alizarin red; therefore, ALNHR refers to the sensor prepared through the non-hydrolytic route and that contained alizarin red as the indicator.

2.3. Cyclic voltammetry and differential pulse voltammetry

Cyclic voltammetry (CV) and differential pulse voltammetry (DPV) measurements were performed using a potentiostat/galvanostat (PARC, model 273) and a conventional three-electrode cell. The silica electrode ($S = 0.152\,cm^2$) with glassy carbon ($S = 0.082\,cm^2$) was used as the working electrode. The working silica electrode consisted of a PVC body containing a graphite disk, which supported the carbon paste. The carbon paste was prepared by mixing highly purified graphite with the modified silica containing alizarin red in an 8:2 (w/w) ratio and a few drops of oil. Ag/AgCl was used as the reference electrode, and a platinum wire was used as the auxiliary electrode. All measurements were carried out in high purity argon. DPV experiments were performed using two media to support the electrolytes: (i) a 0.1 mol L^{-1} $NaBF_4$ solution at pH = 1 and (ii) BR buffer that was prepared by combining acetic acid (pKa = 4.75), phosphoric acid (pKa 2.14, 7.20 and 12.15) and boric acid (pKa = 9.24, 12.74, 13.80) at 0.1 mol L^{-1} each. The pH of the BR buffer solution was adjusted by adding a NaOH solution (1 mol L^{-1} and 0.5 mol L^{-1}) and measured potentiometrically.

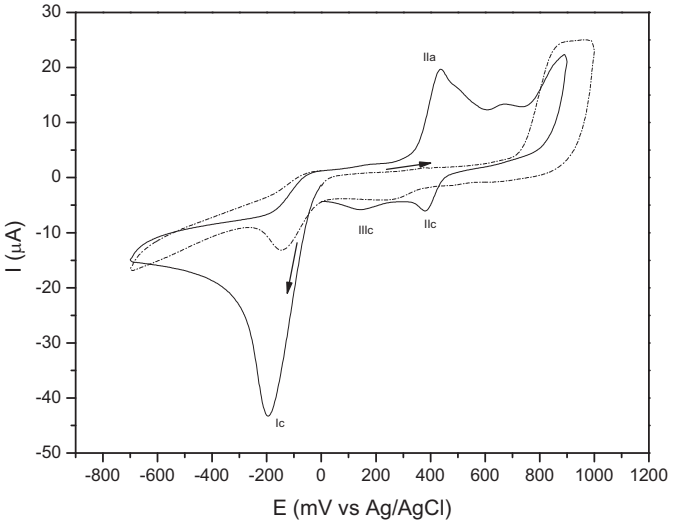

Fig. 1. Cyclic voltammograms of brilliant yellow (BY). Conditions: 1×10^{-3} mol L^{-1} at pH = 3 in a BR buffer solution (υ = 100 mV s^{-1}). (—) Scan to positive *E* and (- -) scan to negative *E*.

2.4. Photoacoustic spectroscopy analysis

A spectrometer manufactured by Optical Properties Laboratory (Physical Institute of UFBA, Brazil) was employed. This instrument bore a halogen lamp (250 W/24 V) source that was mounted at the focus of a concave mirror that projected the filament image into a collimator slit-convergent lens set, generating a parallel beam. The white or polychromatic beam was sent to the monochromator, which was composed of a grating, convergent lens, collimator and output slit. The monochromatic light that emerged from the collimator was intersected by a chopper-type mechanical modulator (SR540 by Stanford) at a frequency of 24 Hz. The angular position of the grating was based on the selected wavelength, determined by a stepper motor and controlled by a purchase and control software. At the end of each mechanical step, the analogical information provided by the light sensors and detected by the SR540 lock-in amplifiers (Stanford Research) was acquired and stored on a personal computer. The spectra were collected within the 300–1800 nm range.

2.5. X-ray photoelectron spectroscopy (XPS)

X-ray photoelectron spectroscopy was performed using an Omicron-SPHERA station using Al Kα radiation (1486.6 eV). The anode was operated at 225 W (15 kV, 15 mA), and the spectra were recorded with a 50 eV pass energy. The detection angle of the photoelectrons (Θ), with respect to the sample surface (take-off angle), was fixed at 53° for all measurements, and the C 1s signal from adventitious carbon at 285 eV was used as an internal energy reference. All spectra were fitted assuming a Shirley background, and all lines were fitted by 70% Gaussian + 30% Lorentzian functions, with set values of full width at half maximum for each line.

3. Results and discussion

The cyclic and differential pulse voltammetry were employed to evaluate the brilliant yellow and acridine sensors behavior, and these electroanalytical techniques were fundamental to confirm dyes encapsulation as well as to propose their interactions with the silica network and to confirm the dyes encapsulation.

Fig. 1 shows the cyclic voltammogram for brilliant yellow in aqueous solution pH = 3, ran in potential range from +1 to −0.7 V *versus* Ag/AgCl at a potential scan rate at 100 mV s^{-1} and 25 °C. When the potential sweep begins at 0.0 V and goes toward the negative potential, a cathodic current peak at −200 mV *versus* Ag/AgCl is observed (Ic). Following the sweep in the positive potential scan direction, an anodic current peak at +380 mV (IIa) and its corresponding anodic current peak at +440 mV (IIc), in the reverse potential sweep, are detected. In addition a cathodic current peak at +145 mV is observed. In the reverse scan the *I–E* profile does not show the pair of current peaks IIa/IIc, and Ic illustrates a low current peak. These results suggest that the electrode process exhibited a redox process with coupled chemical reaction. The electrochemical behavior of brilliant yellow (BY) in terms of electroactive species adsorbed on porous solid matrix has been little investigated. In the literature, the electrochemical properties of brilliant yellow dye immobilized on silica and silica/titania hybrid xerogels containing bridge positively charged 1,4-diazoniabicyclo[2.2.2 octane] was related to E_m (midpoint potential) at +129 mV *versus* ECS in (R_2dabco)BY/SiO_2 (R_2dabco = 1,4-diazoniabicyclo[2.2.2 octane]) [20], probably the current peaks is centered in brilliant yellow. Differential pulse voltammetry was chosen since, in this case, the current peaks intensity were more pronounced than those observed in the cyclic voltammetry.

The pulse voltammograms for brilliant yellow dissolved in aqueous solution at pH 2 (Fig. 2a) is shown to be as complex as those cyclic voltammograms. When the potential sweep begins at −1000 mV and goes toward positive potential, with scan rate 100 mV s^{-1}, anodic current peaks corresponding to cathodic ones (Fig. 2b) are detected at approximately +770 mV (E_{pc1}), +580 mV (E_{pc2}), +390 mV (E_{pc3}) and e −1 mV (E_{pc4}) *versus* Ag/AgCl.

In Ref. [20], (R_2dabco)BY/SiO_2 was evaluated in terms of electrode response depending on the pH values. In the present work, we have observed shifts in the cathodic and anodic current peaks values according to the pH conditions. The analysis of the cathodic current peak (E_{pc}) (Fig. 3) and of the anodic current peak (E_{pa}) at different pH showed a linear correlation (slope around 60 mV). In the case of E_{pc4} × pH curve, the slope is 77 mV, probably due to the occurrence of a coupled reaction, as reflected in the cathodic current peak values (E_{pc}). It is worth noting that in the cyclic voltammogram (see Fig. 1) the difference between anodic current peak IIa and cathodic one IIc is 60 mV, indicating that the redox process involves one electron. In analogy to this current peaks pair, and taking into account that (i) each redox process illustrated in the DPV of dye requires one electron, and (ii) assuming that the concentration ratio between oxidized and reduced species is equal, it can be assumed that E_p/pH is equal to 59 mV, according to the Nernst equation [21]. Thus, the results suggest that each redox process involves one proton. Further studies are necessary to understand thoroughly the involved electrode mechanism of brilliant yellow in aqueous solution. Nevertheless, in the present study it was already possible to realize the suitability of BY as an optical pH sensor.

Fig. 4 shows the DPV of free BY compared to the encapsulated materials that were produced by the three sol–gel routes. For AR, there was a significant change in the curve shape in the 800–100 mV range *versus* Ag/AgCl, and this corresponded to the E_{pc1} and E_{pc2} cathodic processes. The E_{pc3} signal had a decreased current intensity and the E_{pc4} signal was shifted to values that indicated a non-favored reduction. In the anodic scan, the E_{pa3} anodic signal showed an increased current intensity, and the other signal (E_{pa4} investigation at different pH values) showed in the *I–E* profile curves anodic current peak shifts from +430 mV *versus* Ag/AgCl in pH = 2 to approximately +210 mV *versus* Ag/AgCl in pH = 5 (Fig. 5a). Analysis of potential relative values (E_{pa}) as a function of pH, as such showed in solution, illustrated a linear correlation and a slope of 60 mV (Fig. 5b). This behavior might indicate an oxidation process that included the same number of electrons and protons with results equal to one.

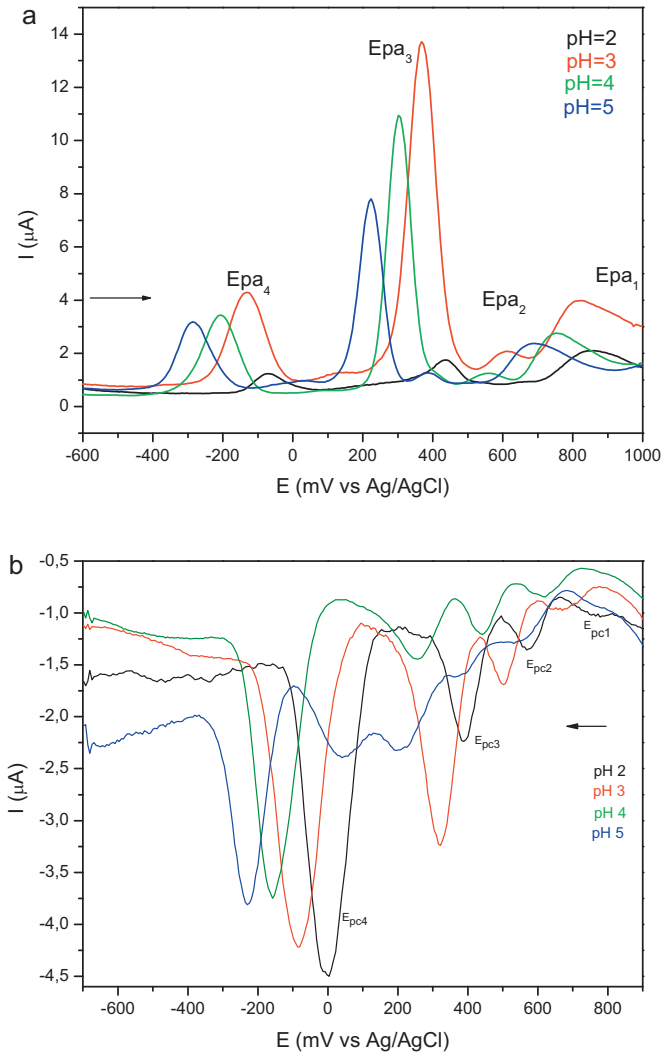

Fig. 2. Differential pulse voltammograms for brilliant yellow (1×10^{-3} mol L^{-1}) in a BR buffer aqueous solution ($v = 100$ mV s^{-1}): (a) anodic scan from a pH range of 2–5; (b) cathodic scan from a pH range of 2–5.

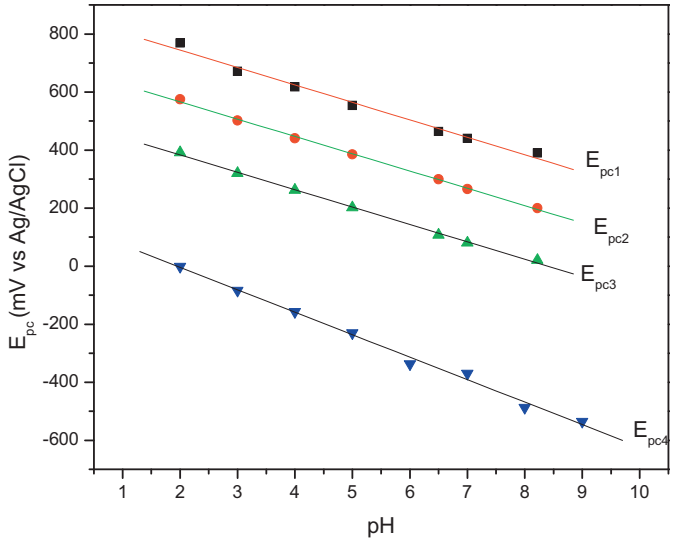

Fig. 3. Linear correlation between E_{pc} *versus* pH.

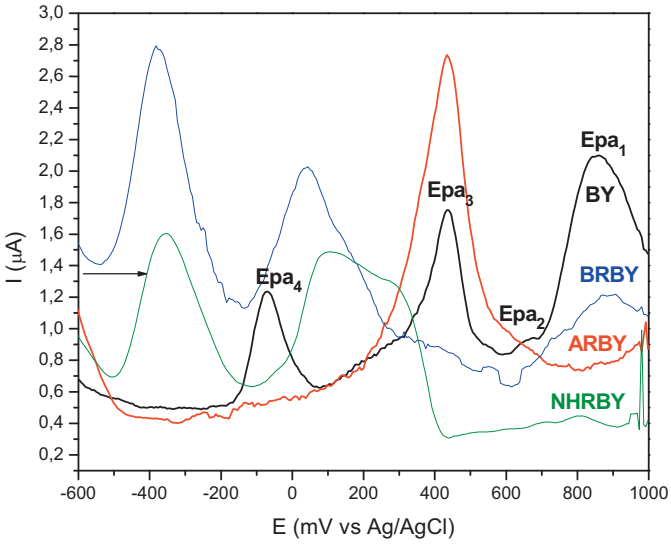

Fig. 4. Differential pulse voltammograms of free BY and the modified electrode with ARBY, BRBY and NHRBY in an aqueous buffer solution at pH = 2. Anodic scan with $v = 100$ mV s^{-1}.

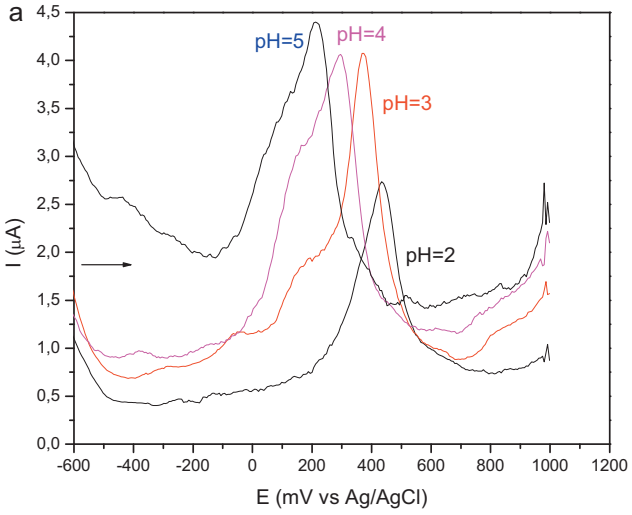

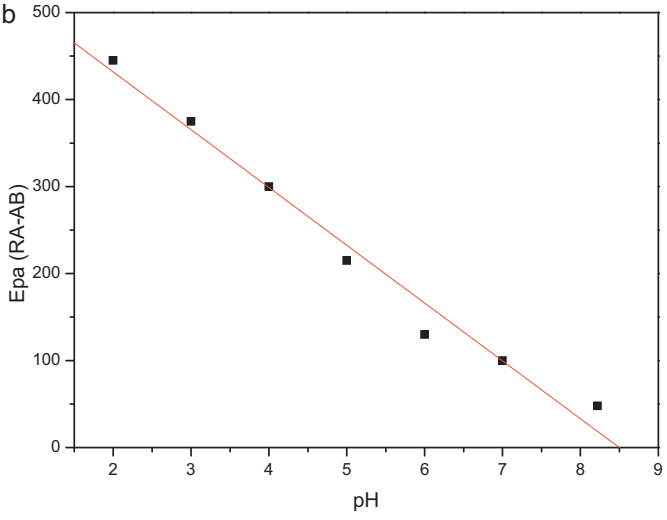

Fig. 5. Differential pulse voltammograms of modified electrode with ARBY in an aqueous buffer solution at pH = 2–5: (a) anodic scan with $v = 100$ mV s^{-1}; (b) linear correlation between E_{pa} *versus* pH.

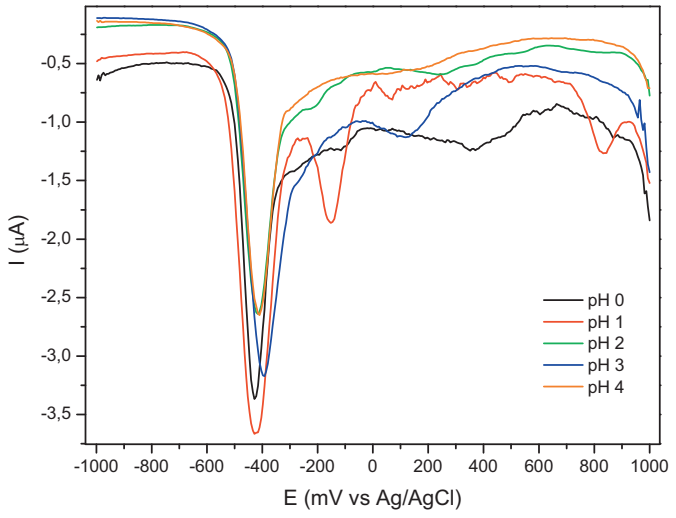

Fig. 6. Differential pulse voltammograms of acridine (1×10^{-3} mol L^{-1}) in an aqueous BR buffer solution ($v = 100$ mV s^{-1}). Cathodic scan in a range of pH from 0 to 4.

As in the case of free BY, DPV for the modified electrode for ARBY and BRBY showed cathodic and anodic current peaks values that were dependent on the pH, and they presented significant potential value shifts when compared to free BY. These results suggested that the silica–pH indicator interaction might produce an intensity signal that could change the electronic density of the pH indicator structure. The pulse voltammograms for BRBY showed shifted signals at different pH values. However, these shifts were not systematic as a function of the pH values, making their interpretation difficult. Nevertheless, the results in these curves supported the proposition of using BRBY as a potential pH sensor.

In the case of the NHRBY sensor, the shape of the cathodic voltammogram showed the same number of reduction processes but with a more pronounced change in the cathodic current peaks (E_{pc3}) cathodic. The anodic scan presented significant changes in the potential range from +200 to −600 mV *versus* Ag/AgCl when compared to free BY. At a different pH, this observed behavior was similar to what was detected in the case of BRBY. However, in the anodic scan, a shift of an anodic signal in the range of +400 to 0 mV was registered, indicating that this system was more prone to oxidation. The obtained results proved the existence of the pH indicators within the silica matrices prepared by all three routes.

3.1. Acridine

In the case of acridine (AC) in an aqueous solution at pH = 1, the voltammogram showed processes centered at +830 mV (E_{pc1}), −150 mV (E_{pc2}), corresponding anodic E_{pa1} and E_{pa2} values, respectively, and E_{pc3} and E_{pa^*} values at −415 mV and +570 mV, respectively (all values relative to the Ag/AgCl reference electrode). The analyses of AC at different pH values showed changes in the shapes of the pulse voltammogram in the range between the E_{pc1} and E_{pc2} signals (Fig. 6). The cathodic signal, E_{pc3}, was slightly shifted from pH = 0 to 1, and a more pronounced modification occurred at pH = 2, illustrating that the reduction became unfavored (*e.g.*, a more negative E_{pc3}). In the pH range of 2–4, the changes were small. The E_{pa1} oxidation process in more acid solutions (pH = 1, approximately +830 mV *versus* Ag/AgCl) showed an increase in current intensity to potential values that were higher than 800 mV, which indicated a less favored acridine oxidation. However, because this evaluation took place in aqueous medium, a conclusive statement was not possible because the scan range could not be extended as a function of the current discharge limitation. Moreover, in the $I \times E$ curve, the E_{pa^*} anodic signal was shifted.

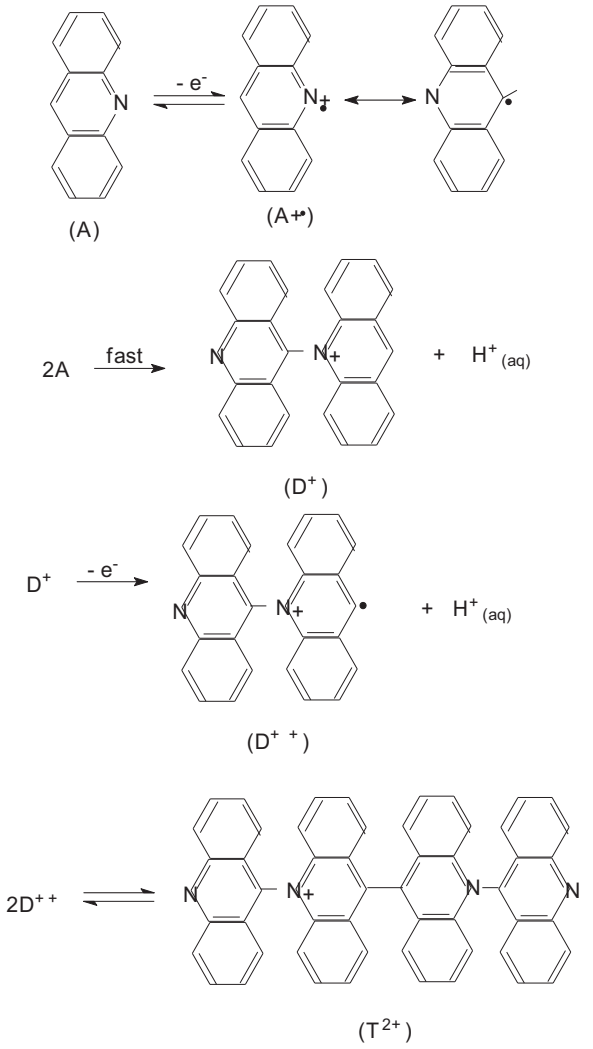

Scheme 2. Acridine oxidation process and coupled reactions [22].

The acridine electrochemical behavior in a non-aqueous solution has been reported in the literature, whereby two oxidation processes have been identified [22]. Investigations on the addition of an acidic aqueous solution led to the proposition that one process corresponded to the acridine oxidation and the other one to its protonation. Therefore, it was proposed that acridine oxidation in aqueous medium was followed by a coupled chemical reaction, and the product of this reaction was a tetramer (Scheme 2) with a cathodic wave around −0.5 V *versus* SCE (saturated calomel electrode). Thus, the E_{pc3} signal could result from acridine oxidation product reduction, and the E_{pa1} signal could result from its oxidation, as shown in Scheme 3: the conversion step from A to A^+.

According to Scheme 3, one mole of hydrogen in protonated form (H^+) is produced and reacts with acridine to form protonated acridine. In the pulse voltammograms in the pH range of 0–4, the E_{pc3} cathodic and E_{pa^*} and E_{pa1} anodic signals shifts could be attributed to the protonation of the acridine pyridine ring (Scheme 3). Studies in a pH range above 4 were limited because of the low solubility of acridine under these conditions.

For the sample of acridine that was encapsulated through the acid route (ARAC), the DPV scan showed current cathodic peaks (Fig. 7) and current anodic peaks correspondent signals that were indicative of pH indicator redox processes, confirming the presence

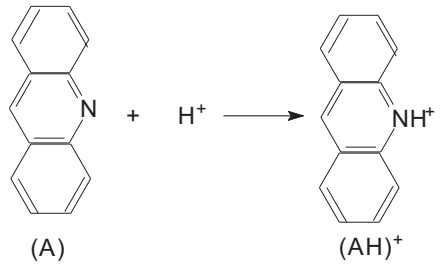

Scheme 3. Acridine protonation.

of the indicator in the material. This behavior was also verified for the other routes. It can be noted that this behavior was evident in materials that lacked the pH indicator (blank), but when obtained by the same routes in the studied potential range, these signals were not present. Like free acridine, DPV of the modified electrodes with the acridine sensors presented anodic and cathodic signals that were pH-dependent and had values that were close to those of the free species. These results confirmed that the silica–pH indicator interactions did not change the electronic density of the pyridine ring, which was the acridine redox center (Scheme 2) [22].

The investigations of ARAC in aqueous solutions at a pH range from 5 to 9 did not show cathodic or anodic signals in the range where the acridine was electroactive, as in the 0–4 pH range. This behavior may suggest that at pH above 5, a chemical reaction resulting in a change for both free and encapsulated acridine took place. This proposition was based on the fact that the encapsulated material, as well as the free indicator, did not have any problems with solubility, and, therefore, the signals should have been present. As described for ARAC, the shape of the BRAC curve indicated the presence of acridine. In this case, structural changes may have occurred during preparation of the sensor (*i.e.*, during the hydrolytic, sol–gel process), once the shape of the final material from DPV in aqueous solution in the 0–4 pH range was similar to that which was detected for ARAC. Therefore, one can state that changes in acridine in aqueous medium were reversible and; moreover, one could infer that the presence of the indicator on the silica surface explained the low interaction between silica and acridine. Like free acridine and ARAC, the BRAC showed pH-dependent, cathodic and anodic signals with similar values. These results suggested that independent

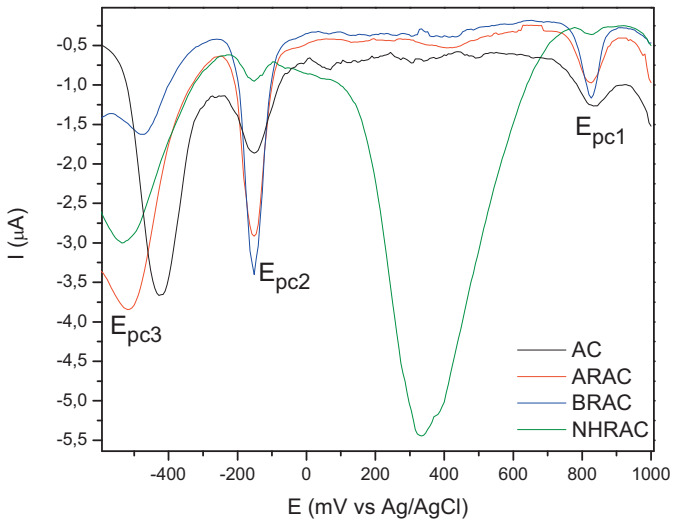

Fig. 7. Differential pulse voltammograms of free AC l (black) and the modified electrode with ARAC, BRAC and NHRAC in an aqueous buffer solution at pH = 1. Cathodic scan with $\nu = 100\,mV\,s^{-1}$.

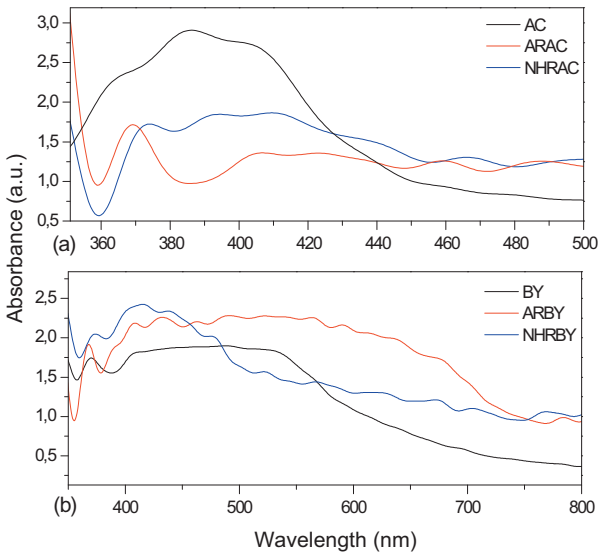

Fig. 8. PAS spectra in the UV–visible region for (a) AC and (b) BY and the corresponding encapsulated sensors that were obtained by AR and NHR.

of the indicator encapsulation route, the interaction with silica was not altered and, therefore, the pulse voltammograms were similar.

The system obtained by NHR (Fig. 7) showed a cathodic signal at +330 mV, which was absent in the voltammograms of free acridine and of the BR system, but in the case of ARAC, this signal was less intense. Additionally, for NHRAC, the DPVs at varying pH were measured, and those results showed signal shifts similar to ARAC. This behavior could indicate a medium dependence for the loss of electrons (Scheme 3).

In an attempt to find more information about the chemical change that acridine seemed to show in its structure under basic conditions, the ARAC was mixed with buffer solutions at varying pH of 1, 5, 7 and 9. After 24 h of magnetic stirring, the solid was collected by filtration. The DPV curve shapes for these different samples showed the same behavior as the ARAC system, thus confirming that the involved chemical process was reversible.

At first, the results of free and encapsulated acridine that had been prepared through the different routes showed that the solid pH sensor prepared by these sol–gel processes could offer a similar response. However, in terms of electrochemical analysis, the acid route seemed to be the most promising one because of its less complex redox mechanism.

Photoacoustic (PAS) analysis also showed different profiles in the spectra that were recorded for the free pH indicator and for the encapsulated sensors (for AC, see Fig. 8a and for BY, see Fig. 8b). As discussed before for the AC sensors, cyclic and pulse voltammetry analysis indicated weak interactions between AC and the silica network. This behavior was in agreement with PAS analysis, and the band shifts could be explained by the protonation of nitrogen in the acridine molecule. Thus, the interactions with the silica network could occur through this site, as is illustrated in Scheme 4a, and seemed to be weak, as discussed in the voltammetric analysis. For the NHRAC, the results could be affected by the presence of the sol–gel process catalyst ($FeCl_3$) residue, which has an intense red color.

According to spectra b of Fig. 8, different band shifts for the BY sensors were also observed: the ARBY sensor showed a broader signal, while the NHRBY sensor showed a narrower one. Generally, the maximum band position of a molecule on the surface of a solid can be affected by several factors, for example: steric effects, medium polarity, hydrogen bond and the surface acidity [23]. In the case of the NHRBY sensor, a hypsochromic shift (blue shift)

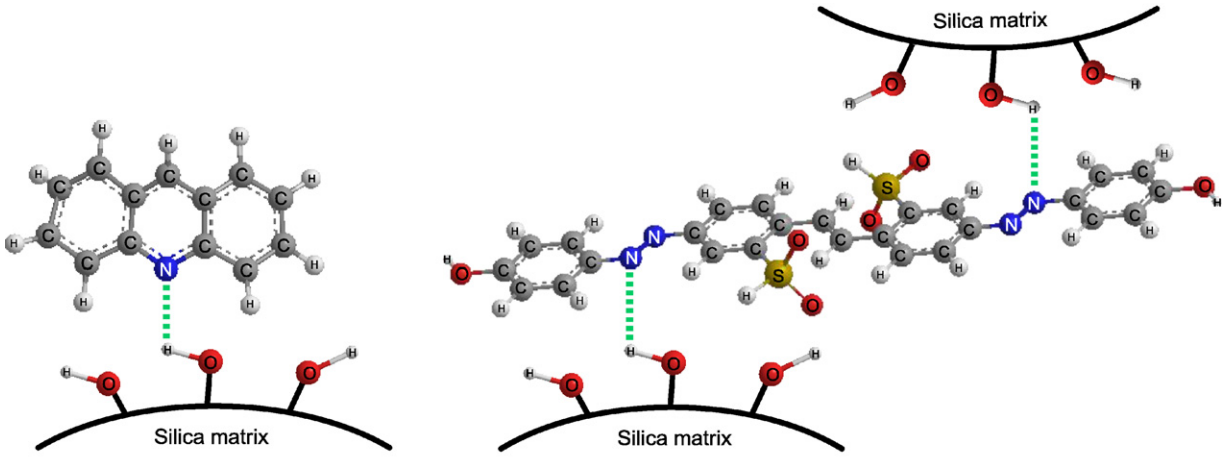

(a) Silica-acridine interaction

(b) AR Silica-brilliant yellow interaction

Scheme 4. Interactions between the silica matrix and pH indicators.

Table 1
Binding energies of the components of the N 1s signal.

	N 1s (1) (eV)	N 1s (2) (eV)
BY	399.7	402.3
ARBY	399.4	401.7
NHRBY	399.8	402.0
BRBY	399.8	402.1

could be observed, and for the ARBY sensor, this shift was broadened. However, for AC, a bathochromic effect was detected in both cases (NHRAC and ARAC), and this behavior could be explained by an increase in medium polarity, which could occur if the indicator interacted with silanol groups of the silica. In this situation, $n–\pi^*$ type transitions tend to be hypsochromic shifts [23], which was the case for BY [4]. On the other hand, $\pi–\pi^*$ transitions tend to have bathochromic effects (red shift) [23], as was observed in the case of the AC transition band. This suggested that nitrogen protonation occurred on the sensor in acid medium [24] (Scheme 4a). For the BR sensors, no bands could be detected for AL or BY, and this was probably due to the low amount of encapsulated indicators.

The systems were further investigated by XPS in an attempt to explain the interactions with the silica network. The analysis for the AC sensors was impossible because the concentration of the pH indicator caused the most plentiful atom (O) signals to be superimposed by the silica signals. However, for the BY sensors, this analysis was possible because of the presence of nitrogen atoms (four units per molecule). The N 1s binding energies for these sensors are shown in Table 1, and the numbers (1) and (2) refer to the two different nitrogens in the BY molecule that were resolved in the XPS spectrum. Every pair of nitrogens (azo group) generated one peak, which could be deconvoluted into two signal contributions that corresponded to each azo nitrogen. Once the BY molecule was symmetric, the two azo groups produced exactly the same signal.

According to Table 1, only the ARBY sensor showed a significant energy shift for the N 1s signals. This result indicated an interaction with the silica network by the azo groups, and it was in agreement with the voltammetry results. Probably, the electronic structure change that was observed by DPV occurred at the azo group nitrogen, which was probably the preferential site for interaction with the silica network, as illustrated in Scheme 4b. For the other routes, energy shifts were not observed at the nitrogen, indicating that the interaction occurred at another chemical group, such as –OH or $–SO_3$. However, one cannot ignore that the molecules exhibiting a stronger interaction, including nitrogen, might be located in silica cavities within deeper layers that could not be detected by XPS, which has a depth penetration in the range of 5 nm.

These results could help to understand the sensors response behavior to the analyte (NH_3 gas), as was reported in a previous study [4]. The interaction of acridine with silica through the pyridinic group (nitrogen protonation) seemed to hinder analyte detection in the AC sensors that showed the longest response times: 135 s (ARAC) and 164 s (NHRAC). In addition, AC lost the ability to change color in solutions at different pH values, which should occur after nitrogen protonation. But, for the ARBY sensor, the interaction with the azo group did not hinder the color changes or the detection of the analyte. Furthermore, this sensor had the shortest response time (98 s). This behavior might indicate that the interaction with the silica network could favor the interaction with the analyte, as a type of activator/promoter on these sites. However, it is important to highlight that these results might also be influenced by the following sensor characteristics: matrix surface area, indicator content and type of sensor, as was reported in a previous paper [4].

4. Conclusions

The present study showed that differential pulse voltammetry is an excellent tool for investigating the interactions of pH indicators within silica networks, and these results agreed with those obtained by complementary techniques such as photoacoustic ultraviolet–visible or X-ray photoelectron spectroscopies. The electrochemical behavior and the pH indicator interactions with the silica network were dependent on the nature of the employed sol–gel route. For the sensors that were prepared with acridine, the interactions with the silica network took place through the nitrogen group from the pyridinic ring, and this behavior was verified by ultraviolet–visible spectroscopy and voltammetry techniques. For the brilliant yellow indicator, different behaviors were observed that were dependent on the route, suggesting different processes during preparation or analysis. For the basic catalyzed and non-hydrolytic routes, it was impossible to uncover a specific interaction. However, for the sensor that had been prepared by the acid route, once the XPS had shown shifts in the nitrogen 1s binding energies, it was concluded that the interaction probably or partially occurred at azo groups.

Acknowledgments

This project was partially financed by the CNPq and FAURGS-Braskem. L.B. Capeletti thanks the CNPq for the grant.

References

[1] R. Buntem, A. Intasiri, W. Lueangchaichaweng, Facile synthesis of silica monolith doped with meso-tetra(p-carboxyphenyl)-porphyrin as a novel metal ion sensor, J. Colloid Interface Sci. 347 (2010) 8–14.
[2] P.C.A. Jeronimo, A.N. Araujo, M. Montenegro, Optical sensors and biosensors based on sol–gel films, Talanta 72 (2007) 13–27.
[3] A. Walcarius, M.M. Collinson, Analytical chemistry with silica sol–gels: traditional routes to new materials for chemical analysis, Annu. Rev. Anal. Chem. 2 (2009) 121–143.
[4] L.B. Capeletti, F.L. Bertotto, J.H.Z. Dos Santos, E. Moncada, M.B. Cardoso, The effect of the sol–gel route on the characteristics of acid–base sensors, Sens. Actuators B 151 (2010) 169–176.
[5] X.Q. Li, J.J. Yuan, H.A. Liu, L. Jiang, S.Q. Sun, S.Y. Cheng, Microgel-silica hybrid particles: strategies for tunable nanostructure, composition, surface property and porphyrin functionalization, J. Colloid Interface Sci. 348 (2010) 408–415.
[6] O.S. Wolfbeis, R. Reisfeld, I. Oehme, Structure and Bonding, 1996.
[7] S. Jurmanovic, S. Kordic, M.D. Steinberg, I.M. Steinberg, Organically modified silicate thin films doped with colourimetric pH indicators methyl red and bromocresol green as pH responsive sol–gel hybrid materials, Thin Solid Films 518 (2010) 2234–2240.
[8] D. Wencel, B.D. MacCraith, C. McDonagh, High performance optical ratiometric sol–gel-based pH sensor, Sens. Actuators B-Chem. 139 (2009) 208–213.
[9] T.M. Butler, B.D. MacCraith, C. McDonagh, Leaching in sol–gel-derived silica films for optical pH sensing, J. Non-Cryst. Solids 224 (1998) 249–258.
[10] Y. Kowada, T. Ozeki, T. Minami, Preparation of silica-gel film with pH indicators by the sol–gel method, J. Sol–Gel Sci. Technol. 33 (2005) 175–185.
[11] H. Segawa, E. Ohnishi, Y. Arai, K. Yoshida, Sensitivity of fiber-optic carbon dioxide sensors utilizing indicator dye, Sens. Actuators B-Chem. 94 (2003) 276–281.
[12] C. Rottman, A. Turniansky, D. Avnir, Sol–gel physical and covalent entrapment of three methyl red indicators: a comparative study, J. Sol–Gel Sci. Technol. 13 (1998) 17–25.
[13] F. Ismail, C. Malins, N.J. Goddard, Alkali treatment of dye-doped sol–gel glass films for rapid optical pH sensing, Analyst 127 (2002) 253–257.
[14] A. Lobnik, N. Majcen, K. Niederreiter, G. Uray, Optical pH sensor based on the absorption of antenna generated europium luminescence by bromothymolblue in a sol–gel membrane, Sens. Actuators B: Chem. 74 (2001) 200–206.
[15] O.B. Miled, H. Ben Ouada, J. Livage, pH sensor based on a detection sol–gel layer onto optical fiber, Mater. Sci. Eng. C-Biomimetic Supramol. Syst. 21 (2002) 183–188.
[16] L.B. Capeletti, I.M. Pepe, Z.N. Rocha, E. Moncada, J.H.Z. dos Santos, Voltammetry of alizarin red species encapsulated within silica matrix, generated by different sol–gel routes, J. Sol–Gel Sci. Technol., submitted for publication.
[17] M.D. Curran, A.E. Stiegman, Morphology and pore structure of silica xerogels made at low pH, J. Non-Cryst. Solids 249 (1999) 62–68.
[18] A. Fisch, C.F. Petry, D. Pozebon, F.C. Stedile, N.S.M. Cardozo, A.R. Secchi, J.H.Z. dos Santos, Immobilization of zirconocene into silica prepared by non-hydrolytic sol–gel method, Macromol. Symp. 245–246 (2006) 77–86.
[19] W. Stober, A. Fink, E. Bohn, Controlled growth of monodisperse silica spheres in micron size range, J. Colloid Interface Sci. 26 (1968) 62–69.
[20] L.T. Arenas, D.S.F. Gay, C.C. Moro, S.L.P. Dias, D.S. Azambuja, T.M.H. Costa, E.V. Benvenutti, Y. Gushikem, Brilliant yellow dye immobilized on silica and silica/titania based hybrid xerogels containing bridged positively charged 1,4-diazoniabicyclo[2.2.2]octane: preparation, characterization and electrochemical properties study, Micropor. Mesopor. Mater. 112 (2008) 273–283.
[21] J.A. Bard, L.R. Faulkner, Electrochemical Methods. Fundamentals and Applications, John Wiley and Sons, New York, 1980.
[22] K. Yasukouchi, I. Taniguchi, H. Yamaguchi, K. Arakawa, Anodic-oxidation of acridine in acetonitrile, J. Electroanal. Chem. 121 (1981) 231–240.
[23] C.N.R. Rao, Ultraviolet and Visible Spectroscopy, Butter-worth, London, 1975.
[24] I. Negron-Encarnacion, R. Arce, M. Jimenez, Characterization of acridine species adsorbed on $(NH_4)_2SO_4$, SiO_2, Al_2O_3, and MgO by steady-state and time-resolved fluorescence and diffuse reflectance techniques, J. Phys. Chem. A 109 (2005) 787–797.